JMEPEG (2011) 20:377–381
DOI: 10.1007/s11665-010-9693-2

1059-9495/$19.00

Effects of Zr Content on the Yield Strength of an Al-Sc Alloy

Min Song, Yuehui He, and Shanfeng Fang

(Submitted March 20, 2010; in revised form April 25, 2010)

The effects of Zr content on the yield strength of an Al-Sc alloy are investigated experimentally. It has been shown that the yield strength increases with time at the beginning of annealing for the investigated one Al-Sc alloy and three Al-Sc-Zr alloys. Such an increase of yield strength results from the high nucleation rate for Al_3Sc particles in Al-Sc alloy and $Al_3(Sc_{1-x},Zr_x)$ particles in Al-Sc-Zr alloys. Throughout the annealing, the yield strength increases with the Zr content, indicating that the alloy with higher Zr content possesses higher yield strength. The high yield strength of the alloy with high Zr content is due to the higher number density and volume fraction of the particles as well as their smaller size and inter-particle spacing. Such a microstructural feature for the particles exhibits a larger Orowan strengthening effect by inhibiting the dislocation movements.

Keywords Al-Sc alloy, microstructure, yield strength, Zr addition

1. Introduction

It has been discovered that the addition of trace amount of Sc and Zr to Al alloys can remarkably improve the mechanical properties of the alloys due to the formation of uniformly distributed secondary $Al_3(Sc_{1-x},Zr_x)$ particles during annealing. These particles can substantially inhibit recrsytallization and pin dislocations (Ref 1-5). Speaking in general, the additions of both Zr and Sc elements into Al alloys have more remarkable effect on the strength of Al alloys than the addition of individual Sc element. The higher yield strength of the Al-Sc-Zr alloys results from the smaller misfit between $Al_3(Sc_{1-x},Zr_x)$ particle and Al matrix as well as the lower growth rate, compared to the Al_3Sc particles.

The structure and morphology of secondary $Al_3(Sc_{1-x},Zr_x)$ particles have extensively been studied (Ref 6-8). Using three-dimensional atom-probe and high resolution transmission microscopy (HRTEM) with EDS microanalysis, Lefebvre et al. (Ref 6), Forbord et al. (Ref 7) and Tolley et al. (Ref 8) showed that $Al_3(Sc_{1-x},Zr_x)$ particles exhibit a complex core-shell structure consisting of an Al_3Sc core embedded in an $Al_3(Sc_{1-x},Zr_x)$ shell. It is believed that this complex core-shell structure is due to the difference in diffusion rates of Sc and Zr in Al matrix. At 300 °C, Sc diffuses four orders of magnitude faster than Zr in Al. Thus, at the beginning of the nucleation process, an intense initial precipitation of Al_3Sc nuclei is favored by fast Sc-diffusion rate in the initial solid solution (Ref 6-8). Then Zr segregates along the interface between Al matrix and the Al_3Sc nuclei to decrease the misfit of the Al_3Sc with the Al matrix. There are several publications in which kinetics and dynamics on the precipitation of $Al_3(Sc_{1-x},Zr_x)$ particles have been experimentally studied and also modeled for binary Al-Sc and Al-Zr (Ref 9-13) and ternary Al-Sc-Zr (Ref 14-17) alloy systems. Using atom-probe tomography, HRTEM, and conventional transmission electron microscopy (TEM), Fuller et al. (Ref 14) found that Sc and Zr partition to $Al_3(Sc_{1-x},Zr_x)$ precipitates, and Zr segregates concomitantly to the α-Al/$Al_3(Sc_{1-x},Zr_x)$ interface. The Zr concentration in the precipitates increases with increasing annealing time. It was also found that the addition of Zr is shown to retard significantly the coarsening rate and stabilize precipitate morphologies (Ref 15).

Up to now, no systematical investigation has been performed on mechanical properties of Al-Sc-Zr alloys, especially the effect of Zr content on the mechanical properties of Al-Sc-Zr alloys. The additions of Zr are known to increase the ambient temperature tensile strength and recrystallization resistance of Al-Sc alloys (Ref 2). Additions of Sc and Zr to some commercial Al alloys have been shown to increase the tensile strength over Zr-free alloys (Ref 18, 19). This effect is attributed to the pining of grain boundaries by highly stable $Al_3(Sc_{1-x},Zr_x)$ particles. Fuller et al. (Ref 19) investigated the mechanical properties (including creep resistance) at room and elevated temperatures for six Al-Sc-Zr alloys and concluded that the microhardness increases with increasing precipitate volume fraction and decreasing average precipitate radius. This study focuses on the effects of Zr content on the tensile yield strength of Al-Sc alloys.

2. Experimental

One Al-Sc binary alloy and three Al-Sc-Zr alloys were investigated in this study. The nominal compositions of the alloys are shown in Table 1. Alloy 1 is a binary Al-Sc alloy, and alloys 2, 3, and 4 are Al-Sc-Zr alloys with various Zr

Min Song, Yuehui He, and **Shanfeng Fang**, State Key Laboratory of Powder Metallurgy, Central South University, Changsha 410083, People's Republic of China. Contact e-mail: min.song.th05@alum.dartmouth.org.

content. The alloys were prepared in an induction furnace in an argon atmosphere by mixing appropriate amounts of Al (99.9%) and master alloys of Al-10 wt.%Zr and Al-2 wt.%Sc. All the alloys were solution treated at 873 K for 72 h, followed by water quenching to the room temperature. The quenched alloys are then annealed at 613 K for various periods of time.

Yield strengths of all the specimens of the annealed alloys were measured at the room temperature. The dog-bone-shaped tensile specimens from all annealed alloys, having a gage size of 6 mm in diameter and 40 mm in length, were subjected to the tensile test at a constant strain rate of 5×10^{-4} s^{-1} on an Instron-8802 testing machine. The yield strength was determined as the 0.2% offset. Each point of the yield strength values has been measured on 5-7 specimens, and the average value of the measurements has been used.

The microstructures of the alloys before and after annealing were observed using optical microscopy and TEM. Thin foils for microstructural characterizations in TEM were prepared by twin jet electro-polishing in a 30% nitric acid and 70% methanol solution at −35 °C and examined in an FEI Tecnai G^2 20 microscopy operating at 200 kV. The size and volume fraction of the precipitates were determined from at least 50 random precipitates seen edge on. Since the radius of the precipitates in the matrix was in the same order as and even greater than the thickness of the thin foil, a correction was employed for differentiating the real dimension from the observed one (Ref 20) and the volume fraction of the precipitates in a thin foil projection was determined by (Ref 21)

$$f_v = \left(\frac{-2\pi r}{\pi r + 4t}\right)\ln(1 - A) \quad \text{(Eq 1)}$$

where r is the radius of the precipitates, t is the foil thickness, and A is the project area fraction of the precipitates, determined by the point count method. The foil thickness was easily obtained by utilizing a grain boundary fringes technique (Ref 22).

Table 1 The nominal composition of the alloys in this study

Alloy	Sc, wt.%, at.%	Zr, wt.%, at.%	Al
Alloy 1	0.39, 0.24	0, 0	Bal.
Alloy 2	0.39, 0.24	0.37, 0.11	Bal.
Alloy 3	0.39, 0.24	0.54, 0.16	Bal.
Alloy 4	0.39, 0.24	0.68, 0.20	Bal.

3. Results

3.1 Microstructure of the As-Quenched Alloys

Figure 1 shows the optical microstructures for the as-quenched alloys. It can be seen that increasing the Zr content can refine the grains. The grain size of binary Al-Sc alloy is ~100 μm, and decreases to ~45, ~40 and ~30 μm when 0.37, 0.54 and 0.68 wt.% Zr contents are added to the alloy, respectively. The most important feature is that increasing the Zr content can remarkably increase the size and number of the primary $Al_3(Sc_{1-x},Zr_x)$ particles formed during solidification since some large-sized primary $Al_3(Sc_{1-x},Zr_x)$ particles can be clearly observed in Zr-containing alloys. It is known that the maximum Sc solid-solubility is about 0.23 at.% (0.38 wt.%) in the primary solid solution (α) at the eutectic temperature of

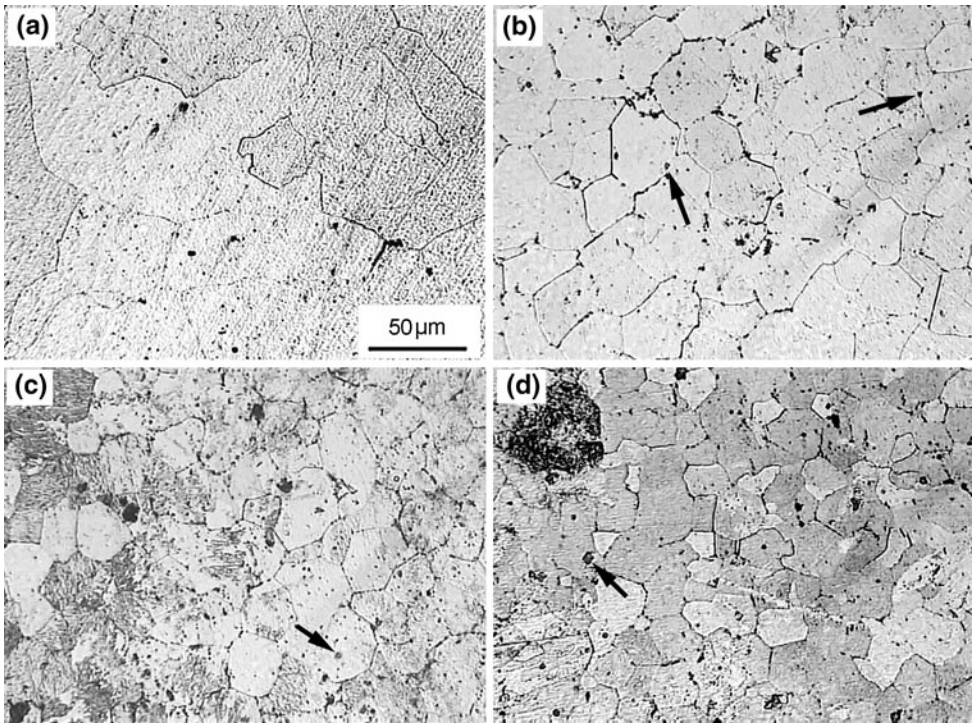

Fig. 1 As-quenching-treated microstructures of (a) alloy 1, (b) alloy 2, (c) alloy 3, and (d) alloy 4. Note that the primary $Al_3(Sc,Zr)$ particles are arrowed

660 °C, while the addition of Zr element will obviously decrease the maximum Sc solid-solubility (Ref 10). Consequently, the primary $Al_3(Sc_{1-x},Zr_x)$ particles can be observed in all the types of alloys with Zr addition because Sc and Zr contents are above solid-solubility limit. It should be noted that the grain refinement with the addition of Zr element is due to the formation of primary $Al_3(Sc_{1-x},Zr_x)$ particles, since this phase can effectively inhibit the grain boundary migration. Thus, the higher the Zr content, the more the primary $Al_3(Sc_{1-x},Zr_x)$ particles and the finer the grain size.

3.2 Microstructure of the Annealed Alloys

Figure 2 shows the TEM microstructures of the prepared alloys after annealing for 5 h at 613 K. It can be seen that the secondary Al_3Sc particles (for alloy 1) and $Al_3(Sc_{1-x},Zr_x)$ (for alloys 2, 3, and 4) distribute uniformly in the matrix after annealing. The size of the particles decreases, and the density and volume fraction of the particles increases with Zr content. This results in a smaller inter-particle spacing between neighboring particles for the alloys with higher Zr content, compared to the alloy with lower Zr content and the binary Al-Sc alloy. Figure 3 shows the experimentally determined average diameter and volume fraction of the precipitates during annealing for the tested four alloys. It can be seen that the size and volume fraction of the particles in the present alloys increase with annealing time up to 70 h. In general, the size of the particles decreases, while the volume fraction of the particles increases with increasing Zr content at any annealing stage, which results in the decrease in the particle interspacing with increasing Zr content. The results further proved that increasing the Zr content can substantially improve the nucleation ratio and decrease the growth velocity of the second phase particles.

3.3 Yield Strength

The dependence of the yield strength on the annealing time was experimentally measured, as shown in Fig. 4. It can be seen that the yield strength increases dramatically with time at the beginning of annealing for all the four types of the alloys. After annealing for about 20 h, the increasing velocity decreases and the yield strength remains almost constant. It should be noted that at any stage of annealing, the yield strength increases with the Zr content, which indicates that the alloy with higher Zr content has the higher yield strength.

4. Discussion

It has been shown in Fig. 4 that increasing the Zr content leads to the increase of the yield strength for the investigated alloys throughout the annealing. Two possible reasons can be used to explain this phenomenon. First, the increase of the yield strength is attributed to the grain refinement. It can be seen from Fig. 1 that increasing Zr content can substantially decrease the grain size of the alloys, and this improves the yield strength according to Hall-Petch relationship. Second, the high yield strength of the alloy with high Zr content is due to the smaller size and larger density of the $Al_3(Sc_{1-x},Zr_x)$ particles, which

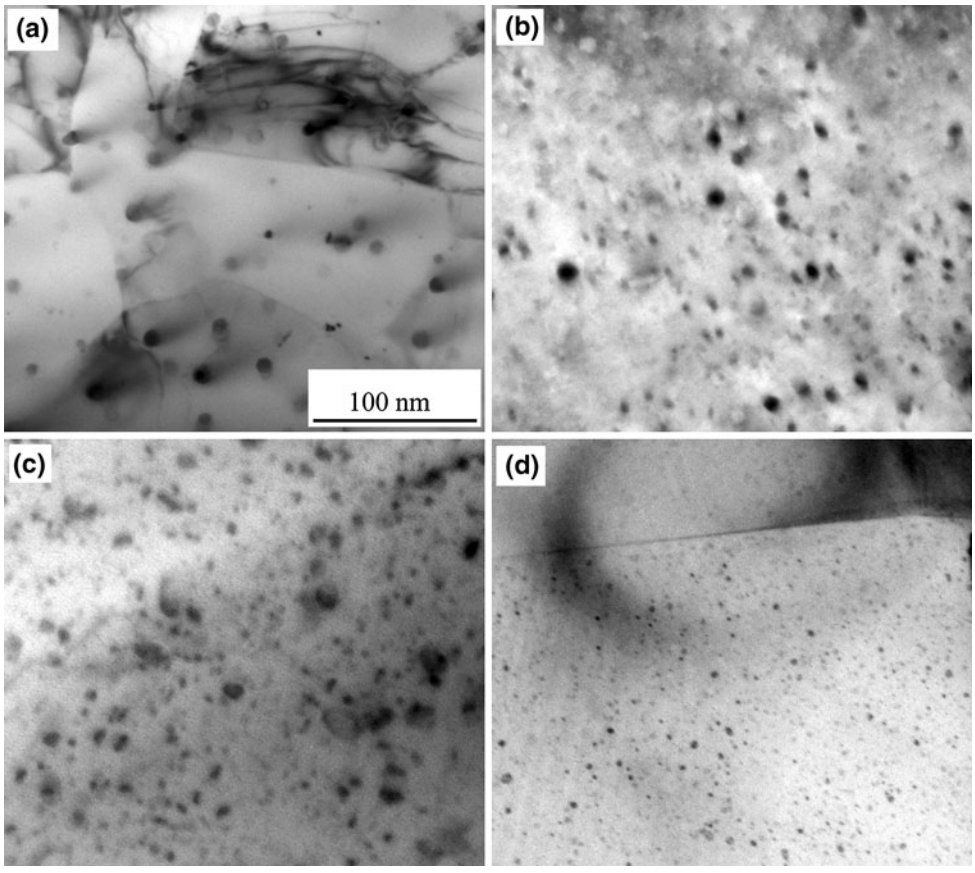

Fig. 2 TEM microstructures of (a) alloy 1, (b) alloy 2, (c) alloy 3 and (d) alloy 4 after annealing at 613 K for 5 h

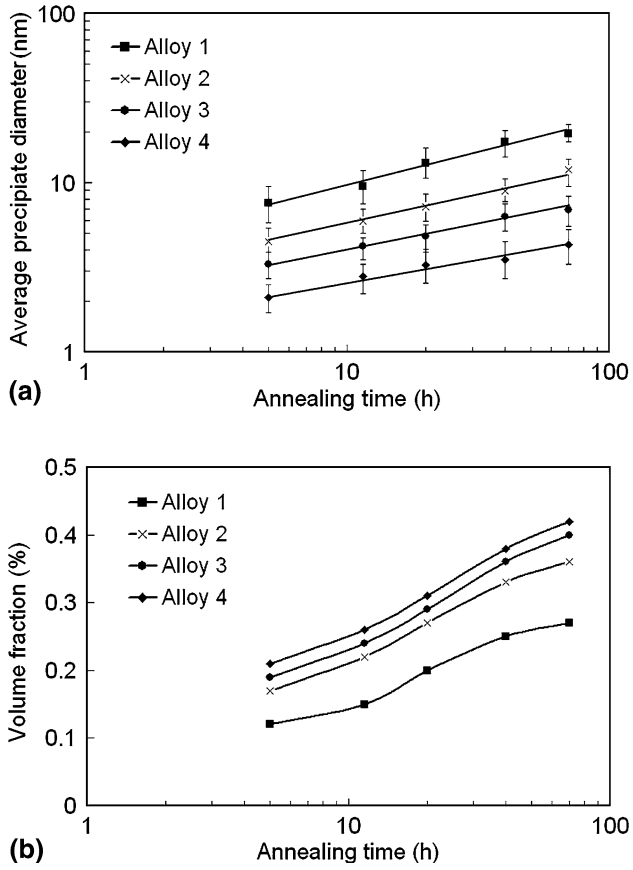

Fig. 3 Particle (a) average diameter and (b) volume fraction evolutions with annealing time

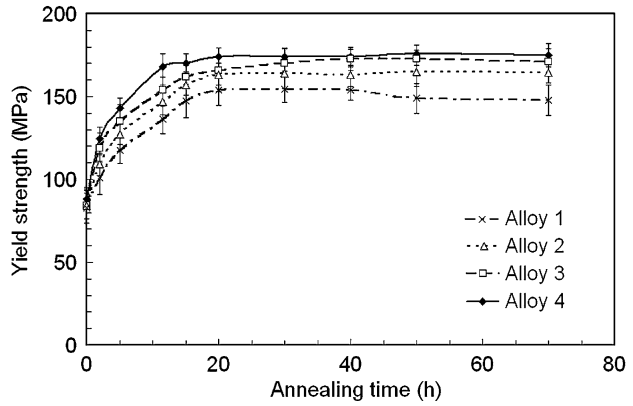

Fig. 4 Yield strength evolutions of four types of alloys

results in a smaller inter-particle spacing. It is widely accepted that the contributions of the yield strength of the Al-Sc-Zr alloys includes the matrix intrinsic strength, solution strength, and particle strength. In this study, the solution strengths are from Sc and Zr solid solutions in the matrix, while the particle strength results from the inhibition of the dislocation movements by $Al_3(Sc_{1-x},Zr_x)$ particles in Al-Sc-Zr alloys or Al_3Sc particles in Al-Sc alloy (Orowan mechanism). Figure 5 shows a strong interaction between secondary $Al_3(Sc,Zr)$ particles and dislocations (arrowed) in alloy 4 after annealed for 40 h and tensile testing. It can be seen from Fig. 5 that a large number of the dislocations have been pinned by the $Al_3(Sc_{1-x},Zr_x)$

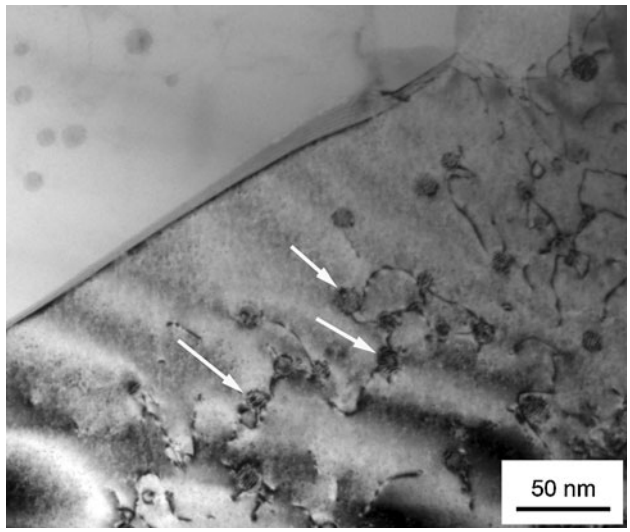

Fig. 5 The interaction between secondary $Al_3(Sc,Zr)$ particles and dislocations in alloy 4 (arrowed, after annealing for 40 h and tensile testing)

particles during deformation, which substantially improve the yield strength. Based on a previous study (Ref 23), the increase in the yield strength due to the Orowan strengthening, $\Delta\sigma_{Or}$, can be expressed by

$$\Delta\sigma_{Or} = KM(1-\upsilon)^{-0.5}(Gb/\lambda)\ln(r/b) \quad \text{(Eq 2)}$$

where M is the Taylor factor, υ is the matrix Poisson's ratio, G is the matrix shear modulus, b is the magnitude of the Al matrix Burgers vector, K is a constant which depends on the particle size distribution, r is the mean particle radius on the dislocation slip plane, and λ is an effective inter-particle spacing on the dislocation slip plane.

From Eq 2, we know that decreasing the inter-particle spacing or increasing the particle diameter can increase the yield strength. The relationship between the inter-particle spacing and particle diameter can be expressed as

$$\varphi = 2\pi Sr^3/\lambda^3 \quad \text{(Eq 3)}$$

where φ is the volume fraction of the particles and S is the shape factor (aspect ratio) and equals 1 for spherical particles. Substituting Eq 3 into Eq 2, we have

$$\Delta\sigma_{Or} = KM(1-\upsilon)[Gb\varphi^{1/3}/r(2\pi S)^{1/3}]\ln(r/b) \quad \text{(Eq 4)}$$

Equation 4 indicates that a smaller particle size and larger volume fraction of the particles will result in a larger increase in the yield strength by Orowan mechanism. In this study, the volume fraction and density of the particles are larger, and the size of the particles is smaller for the alloys with higher Zr content in any annealing stage, as shown in Fig. 3, resulting in a larger Orowan strength effect during the entire annealing stage up to 70 h. Figure 6 shows the dependence of the yield strength on the average inter-particle pacing for all the tested alloys. The particle interspacing was calculated using Eq 3 and the data from Fig. 3. It can be seen from Fig. 6 that the yield strength decreases as the inter-particle spacing increases, which agrees well with the Orowan strengthening mechanism since smaller inter-particle spacing results in a larger shear stress to push the dislocations bypassing the particles, as shown in Eq 2 and 4.

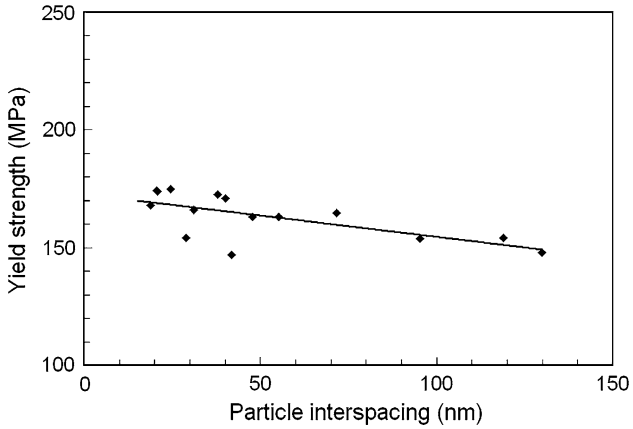

Fig. 6 Yield strength as a function of the inter-particle spacing

In general, the addition of Zr element will obviously decrease the maximum Sc solid solubility and increase the supersolid-solution degree, which can increases the nucleation driving force and nucleation ratio at the subsequent annealing process (Ref 10). Thus, the nucleation ratio of $Al_3(Sc_{1-x},Zr_x)$ particles is larger than Al_3Sc particles with the same Sc concentration. After nucleation, the coarsening speed of $Al_3(Sc_{1-x},Zr_x)$ particles is slower than Al_3Sc particles, resulting from smaller mismatch between the particles and Al matrix by the addition of Zr, and the inhibition of the Sc diffusion to the particles by Zr-rich shell around the Al_3Sc nuclei. At the beginning of the nucleation process, an intense initial precipitation of Al_3Sc nuclei is favored by fast Sc-diffusion rate in the initial solid solution. Then Zr segregates along the interface between Al matrix and the Al_3Sc nuclei to decrease the misfit of the Al_3Sc with the Al matrix. Previous studies (Ref 6-8) showed that $Al_3(Sc_{1-x},Zr_x)$ particles exhibit a complex core-shell structure consisting of an Al_3Sc core embedded in an $Al_3(Sc_{1-x},Zr_x)$ shell. The segregation of Zr on the interface of the particles substantially inhibit the diffusion of the Sc atoms form the Al matrix to the particles, thus, decreases the coarsening speed of the $Al_3(Sc_{1-x},Zr_x)$ particles.

5. Conclusion

In this study, the effect of Zr content on the yield strength and microstructure of Al-Sc alloys has been studied. It has been shown that the second phase particle in the alloy with higher Zr content has larger nucleation ratio and slower coarsening speed, which result in smaller size and inter-particle spacing, and larger density and volume fraction of the particles. The alloy with higher Zr content exhibits a larger Orowan strength effect by inhibiting the dislocation movements. As a result of the microstructures, the yield strength of the alloy increases as the Zr content increases throughout the annealing, indicating that the alloy with higher Zr content has higher yield strength.

Acknowledgments

This study was financially supported by the National Natural Science Foundation of China (50831007, 50823006 and 50825102) and the Chinese Postdoctoral special Science Foundation (200801345).

References

1. V. Singh, D.V.A. Rao, and A.A. Gokhale, Potential of Scandium Additions in Developing New Aluminium Based Cast Alloys, *Indian Foundry J.*, 2004, **50**, p 44–48
2. C.B. Fuller, D.N. Seidman, and D.C. Dunand, Mechanical Properties of Al(Sc,Zr) Alloys at Ambient and Elevated Temperatures, *Acta Mater.*, 2003, **51**, p 4803–4814
3. Y.W. Riddle, H. Hallem, and N. Ryum, Highly Recrystallization Resistant Al-Mn-Mg Alloys Using Sc and Zr, *Mater. Sci. Forum*, 2002, **396–402**, p 563–568
4. O.N. Senkov, R.B. Bhat, S.V. Senkova, and J.D. Schloz, Microstructure and Properties of Cast Ingots of Al-Zn-Mg-Cu Alloys Modified with Sc and Zr, *Metall. Mater. Trans. A*, 2005, **36**, p 2115–2126
5. K.L. Kendig and D.B. Miracle, Strengthening Mechanisms of an Al-Mg-Sc-Zr Alloy, *Acta Mater.*, 2004, **50**, p 4165–4174
6. W. Lefebvre, F. Danoix, H. Hallem, B. Forbord, A. Bostel, and K. Marthinsen, Precipitation Kinetic of $Al_3(Sc,Zr)$ Dispersoids in Aluminium, *J. Alloys Compd.*, 2009, **470**, p 107–110
7. B. Forbord, W. Lefebvre, F. Danoix, H. Hallem, and K. Marthinsen, Three Dimensional Atom Probe Investigation on the Formation of $Al_3(Sc,Zr)$-Dispersoids in Aluminium Alloys, *Scr. Mater.*, 2004, **51**, p 333–337
8. A. Tolley, V. Radmilovic, and U. Dahmen, Segregation in $Al_3(Sc,Zr)$ Precipitates in Al-Sc-Zr Alloys, *Scr. Mater.*, 2005, **52**, p 621–625
9. H.H. Jo and S.I. Fujikawa, Kinetics of Precipitation in Al-Sc Alloys and Low Temperature Solid Solubility of Scandium in Aluminium Studied by Electrical Resistivity Measurements, *Mater. Sci. Eng. A*, 1993, **171**, p 151–161
10. R.W. Hyland, Homogeneous Nucleation Kinetics of Al_3Sc in a Dilute Al-Sc Alloy, *Metall. Trans. A*, 1992, **23**, p 1947–1955
11. C. Watanabe, T. Kondo, and R. Monzen, Coarsening of Al_3Sc Precipitates in an Al-0.28 wt Pct Sc Alloy, *Metall. Mater. Trans. A*, 2004, **35**, p 3003–3008
12. J. Royset and N. Ryum, Kinetics and Mechanisms of Precipitation in an Al-0.2 wt.%Sc Alloy, *Mater. Sci. Eng. A*, 2005, **396**, p 409–422
13. K.E. Knipling, D.C. Dunand, and D.N. Seidman, Nucleation and Precipitation Strengthening in Dilute Al-Ti and Al-Zr Alloys, *Metall. Mater. Trans. A*, 2007, **38**, p 2552–2563
14. C.B. Fuller, J.L. Murray, and D.N. Seidman, Temporal Evolution of the Nanostructure of Al(Sc,Zr) Alloys. Part I. Chemical Compositions of $Al_3(Sc_{1-x}Zr_x)$ Precipitates, *Acta Mater.*, 2005, **53**, p 5401–5413
15. C.B. Fuller and D.N. Seidman, Temporal Evolution of the Nanostructure of Al(Sc,Zr) Alloys. Part II. Coarsening of $Al_3(Sc_{1-x}Zr_x)$ Precipitates, *Acta Mater.*, 2005, **53**, p 5415–5428
16. E. Clouet, A. Barbu, L. Lae, and G. Martin, Kinetics of Al_3Zr and Al_3Sc in Aluminum Alloys Modeled with Cluster Dynamics, *Acta Mater.*, 2005, **53**, p 2313–2325
17. E. Clouet, L. Lae, T. Epicier, W. Lefebvre, M. Nastar, and A. Deschamps, Complex Precipitation Pathways in Multicomponent Alloys, *Nat. Mater.*, 2006, **5**, p 482–488
18. O.N. Senkov, M.R. Shagiev, S.V. Senkova, and D.B. Miracle, Precipitation of $Al_3(Sc,Zr)$ Particles in an Al-Zn-Mg-Cu-Sc-Zr Alloy During Conventional Solution Heat Treatment and Its Effect on Tensile Properties, *Acta Mater.*, 2008, **56**, p 3723–3738
19. C.B. Fuller, A.R. Krause, D.C. Dunand, and D.N. Seidman, Microstructure and Mechanical Properties of a 5754 Aluminum Alloy Modified by Sc and Zr Additions, *Sci. Eng. A*, 2002, **338**, p 8–16
20. J.M.G. Crompton, R.M. Waghorne, and C.B. Brook, The Estimation of Size Distribution and Density of Precipitates from Electron Micrographs of Thin Foils, *Br. J. Appl. Phys.*, 1966, **17**, p 1301–1305
21. D.L. Gilmore and R.M. Starker, Jr., Trace Element Effects on Precipitation Processes and Mechanical Properties in an Al-Cu-Li Alloy, *Metall. Mater. Trans. A*, 1997, **28**, p 1399–1415
22. J.W. Edington, *Practical Electron Microscopy in Materials Science*, Von Norstrand Reinhold Company, London, 1976, p 207
23. M.F. Ashby, *Strengthening Methods in Crystals*, Elsevier, New York, 1971, p 165–171